CRYSTAL GROWTH & DESIGN

Article

Cite This: *Cryst. Growth Des.* 2018, 18, 5155−5165

pubs.acs.org/crystal

Structural Versatility of 3*d*-Ce^{III} Heterometallic Coordination Polymers Using Co^{II} or Cu^{II}

Carlos Cruz,[†,‡] Evgenia Spodine,[‡,§] Nathalie Audebrand,[∥] Diego Venegas-Yazigi,[‡,⊥] and Verónica Paredes-García*[,†,‡]

[†]Universidad Andres Bello, Facultad de Ciencias Exactas, Departamento de Ciencias Químicas, Santiago, Chile

[‡]CEDENNA, Santiago, Chile

[§]Universidad de Chile, Facultad de Ciencias Químicas y Farmacéuticas, Departamento de Química, Santiago, Chile

[∥]Univ Rennes, CNRS, ISCR (Institut des Sciences Chimiques de Rennes) - UMR 6226, F-35000, Rennes, France

[⊥]Universidad de Santiago de Chile, Facultad de Química y Biología, Departamento de Ciencias de los Materiales, Santiago, Chile

Supporting Information

ABSTRACT: In the present work, we report the synthesis and characterization of two new heterometallic coordination polymers based on Ce^{III} and containing Co^{II} or Cu^{II} cations, assembled by the bifunctional ligand 1*H*-imidazole-4,5-dicarboxylic acid, $[Ce(H_2O)_2(HIDC)Co(IDC)]\cdot H_2O$ **CoCe** and $[Ce(H_2O)_2(H_2IDC)Cu(H_2O)(IDC)Cu_{0.2}(H_{1.6}IDC)]$ **CuCe**. Compound **CoCe** was obtained under one pot hydrothermal synthesis, while **CuCe** was synthesized by a step-by-step synthesis using the metalloligand $[Cu(H_2IDC)_2(H_2O)_2]$ **Cu1**, as precursor. From a structural point of view, **CoCe** presents an intrincated 3D structure, in which alternating Λ-Δ chiral Co^{II} chains can be observed, which are assembled by discrete Ce^{III} fragments, giving rise to the 3D structure. Meanwhile, **CuCe** presents a structure formed by $[Cu_2Ce_2]$ heterometallic chains, partially assembled by Cu^{II} cations in a 2D structure. Magnetic properties reveal that both **CoCe** and **CuCe** present a global antiferromagnetic behavior, dominated by the interaction between Co^{II}-Co^{II} or Cu^{II}-Cu^{II} entities connected by μ^2-κ*N*,*O*-κ*O*′′′,*N*′ bridges, belonging to H_3IDC anionic derivatives. Moreover, a weak ferromagnetic phenomenon was found in compound **CoCe**, corroborated by hysteresis loops and *ac* magnetization.

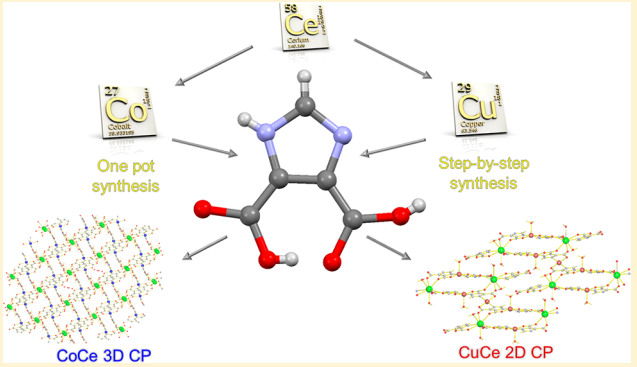

1. INTRODUCTION

In the field of material science, the new technologies drive the innovation in the synthesis and characterization of different kinds of novel materials. In this sense, the coordination polymers (CPs) are one of the most studied materials. The interest in this kind of compounds lies in that a combination of different metal centers with a proper ligand can afford an infinity of new structures, with novel architectures and topologies. Homometallic CPs have been extensively studied in fields such as luminescent sensors,[1,2] magnetic materials,[3,4] gas separation,[5,6] semiconductor materials,[7] and heterogeneous catalysts.[8] On the other hand, researches on CPs that combine more than one different kind of metal cations are still less exploited. For example, heterometallic coordination polymers (HCP) based on 3*d* and 4*f* cations have become attractive in recent years, principally due to the differences on the coordination features which permit obtaining sophisticated structures and novel properties. For example, Jin et al. reported the synthesis of two 3D frameworks $[Pr_2Cu_5I_4(IN)_7\cdot(H_2O)_2\cdot(solv)]_n$ (solv = benzene or toluene) using isonicotinic acid (HIN). These Pr^{III}-Cu^{I} compounds showed a high framework stability and reversible solvent exchange, but the most important feature was that both compounds presented chiral structures, these obtained from a symmetrical ligand.[9] On the other hand, using pyrazine-2,3-dicarboxylic acid (H_2pzdc), Yang et al. obtained a series of 3*d*-4*f* 2D networks $[Ln_2Co(pzdc)_4(H_2O)_6]\cdot 2H_2O$ (Ln = La^{III}, Pr^{III}, Eu^{III}, and Gd^{III}) that were used as catalysts in the synthesis of cyanohydrin. These compounds showed very high conversions for benzaldehyde and high selectivity to cyanohydrin at room temperature in solvent free conditions.[10] Zhang et al. presented an excellent example of multifunctional materials in a family of isostructural 3D compounds $[LnZnL(CO_3)_2(H_2O)]$ (Ln = Eu^{III}, Gd^{III}, Dy^{III}, Ho^{III}, Er^{III}, Tm^{III}, Yb^{III}, Lu^{III}; L = 4′-(4-carboxyphenyl)-2,2′:6′,2″-terpyridine). Structurally, all the compounds presented interpenetrated and chiral structures. Moreover, compound Eu^{III}Zn^{II} presented potential applications in luminescent sensing of nitrobenzene, while the

Received: April 18, 2018
Revised: July 13, 2018
Published: July 19, 2018

DOI: 10.1021/acs.cgd.8b00590
Cryst. Growth Des. 2018, 18, 5155−5165

Table 1. Crystal Data and Structure Refinement for CoCe and CuCe

	CoCe	CuCe
empirical formula	$CoCeC_{10}H_9N_4O_{11}$	$Cu_{1.2}CeC_{15}H_{12.6}N_6O_{15}$
formula weight	560.28	751.78
temperature/K	296.15	150.15
crystal system	monoclinic	monoclinic
space group	$P2_1/n$	$P2_1/n$
a/Å	9.213(6)	11.0696(4)
b/Å	10.081(6)	6.9284(2)
c/Å	17.456(11)	26.1233(8)
α/deg	90	90
β/deg	98.777(7)	95.6510(10)
γ/deg	90	90
volume/Å^3	1602.2(17)	1993.78(11)
Z	14	8
ρ_{calc}/g/cm^3	2.3117	2.435
μ/mm^{-1}	3.912	3.595
F(000)	1068.5	1426.0
radiation	Mo Kα (λ = 0.71073)	Mo Kα (λ = 0.71073)
2Θ range for data collection/deg	4.68−60.82	5.688−55.132
index ranges	$-11 \le h \le 13$, $-14 \le k \le 14$, $-24 \le l \le 24$	$-14 \le h \le 14$, $-9 \le k \le 9$, $0 \le l \le 33$
reflns collected	26319	8609
independent reflns	4573 [R_{int} = 0.1126, R_{sigma} = 0.0819]	4561 [R_{int} = 0.0224, R_{sigma} = 0.0376]
data/restraints/parameters	4573/2/267	4561/4/398
goodness-of-fit on F^2	1.025	1.098
final R indexes [$I \ge 2\sigma(I)$]	R_1 = 0.0525, wR_2 = 0.1104	R_1 = 0.0237, wR_2 = 0.0454
final R indexes [all data]	R_1 = 0.0810, wR_2 = 0.1277	R_1 = 0.0302, wR_2 = 0.0467
largest diff. peak/hole/e Å^{-3}	1.77/−1.85	0.59/−0.77
	#1 = $-x$, $3-y$, $1-z$; #2 = $-x$, $2-y$, $1-z$; #3 = $-1+x$, $1+y$, $+z$; #4 = $1/2-x$, $1/2+y$, $3/2-z$; #5 = $1-x$, $2-y$, $1-z$; #6 = $3/2-x$, $1/2+y$, $3/2-z$; #7 = $3/2-x$, $-1/2+y$, $3/2-z$	#1 = $+x$, $-1+y$, $+z$; #2 = $+x$, $1+y$, $+z$; #3 = $1-x$, $1-y$, $1-z$; #4 = $-1+x$, $-2+y$, $+z$; #5 = $-x$, $-y$, $1-z$; #6 = $-x$, $-1-y$, $1-z$

$Gd^{III}Zn^{II}$ framework allowed one to quantify the magnetic interactions between Gd^{III} ions, by the calculation of the coupling constant.[11]

The presence of two different metal cations in this type of 3*d*-4*f* materials adds structural complexity and gives the possibility of obtaining new functionalities. As the hardness of both cations is different, the use of an N,O-bifunctional ligand seems to be the most reasonable strategy for the rational design of heterometallic CPs,[12−14] since 3*d* cations can bind either N or O atoms, while 4*f* centers are strongly oxophilic according to the Pearson HSAB theory.[15] For this reason, the 1*H*-imidazole-4,5-dicarboxylic acid attracted our attention, due to (a) the existence of both a N-heterocyclic ring from imidazole and carboxylate functionalities, (b) the ability to generate different anionic species, in order to balance the positive charge, and (c) the existence of multiple coordination modes, among others.[16,17] Although H_3IDC has been previously used as a building block for the 3*d*-4*f*,[18−21] its rich coordination chemistry still makes this organic linker an exceptional candidate to be used in the construction of new 3*d*-4*f* HCPs. In the present work, we report the synthesis, structural and magnetic characterization of two new 3*d*-Ce^{III} HCPs (3*d* = Co^{II} or Cu^{II}), $[Ce(H_2O)_2(HIDC)Co(IDC)]\cdot H_2O$ **CoCe** and $[Ce(H_2O)_2(H_2IDC)Cu(H_2O)(IDC)Cu_{0.2}(H_{1.6}IDC)]$ **CuCe**, which were obtained under hydrothermal conditions using one pot and step-by-step synthesis for **CoCe** and **CuCe**, respectively.

2. EXPERIMENTAL SECTION

2.1. Synthesis of $[Ce(H_2O)_2(HIDC)Co(IDC)]\cdot H_2O$ (CoCe). A suspension of H_3IDC (0.3 mmol), $Co(NO_3)_2\cdot 6H_2O$ (0.3 mmol), and $Ce(acac)_3$ (0.3 mmol) (acac = acetylacetonate) was placed in a 23 mL Teflon-lined stainless-steel autoclave vessel with 10 mL of water and heated at 150 °C for 5 days, under self-generated pressure. The reaction mixture was cooled down to room temperature. Fuchsia prismatic crystals of **CoCe**, stable and suitable for X-ray diffraction, were separated by filtration. MW: 560.28 g/mol. Yield of 50%, based on the lanthanide salt. Analysis calculated for $CoCeC_{10}H_9N_4O_{11}$ (%): C, 21.44; H, 1.62; N, 10.00. (%) Found: C, 21.28; H, 1.73; N, 9.65.

2.2. Synthesis of $[Ce(H_2O)_2(H_2IDC)Cu(H_2O)(IDC)Cu_{0.2}(H_{1.6}IDC)]$ (CuCe). Compound **CuCe** was obtained in a two-step reaction, using $[Cu(H_2IDC)_2(H_2O)_2]$ (**Cu1**), as metalloligand. **Cu1** was synthesized by a 2 h reflux of a solution of $Cu(NO_3)_2\cdot 3H_2O$ (5 mmol) and H_3IDC (10 mmol) in 30 mL of water. (MW: 409.79 g/mol. Yield of 89%, based on the copper salt). Analysis calculated for $CuC_{10}H_{10}N_4O_{10}$ (%): C, 29.32; H, 2.44; N, 13.67. (%) Found: C, 30.15; H, 2.46; N, 13.77. A suspension of **Cu1** (0.15 mmol), $Ce(NO_3)_2\cdot 3H_2O$ (0.10 mmol) and $K_2C_2O_4\cdot H_2O$ (0.10 mmol) was placed in a 23 mL Teflon-lined stainless-steel autoclave vessel with 10 mL of water and heated at 120 °C under self-generated pressure for 5 days. The reaction mixture was cooled down to room temperature in 16 h. Light blue stick crystals of **CuCe**, stable and suitable for X-ray diffraction, were separated by filtration. MW: 735.959 g/mol. Yield of 51%, based on lanthanide salt. Analysis calculated for $Cu_{1.2}CeC_{15}H_{12.6}N_6O_{14}$ (%): C, 23.96; H, 1.74; N, 11.42. (%) Found: C, 23.47; H, 1.78; N, 10.66.

2.3. X-ray Data Collection and Structure Determination. A single crystal of **CoCe** was directly picked up and glued on a glass capillary using epoxy resin. Scans on a Bruker APEXII diffractometer confirmed enough crystal quality to perform full recording data at room temperature. X-ray radiation of Mo−Kα (λ = 0.71073 Å) was

DOI: 10.1021/acs.cgd.8b00590
Cryst. Growth Des. 2018, 18, 5155−5165

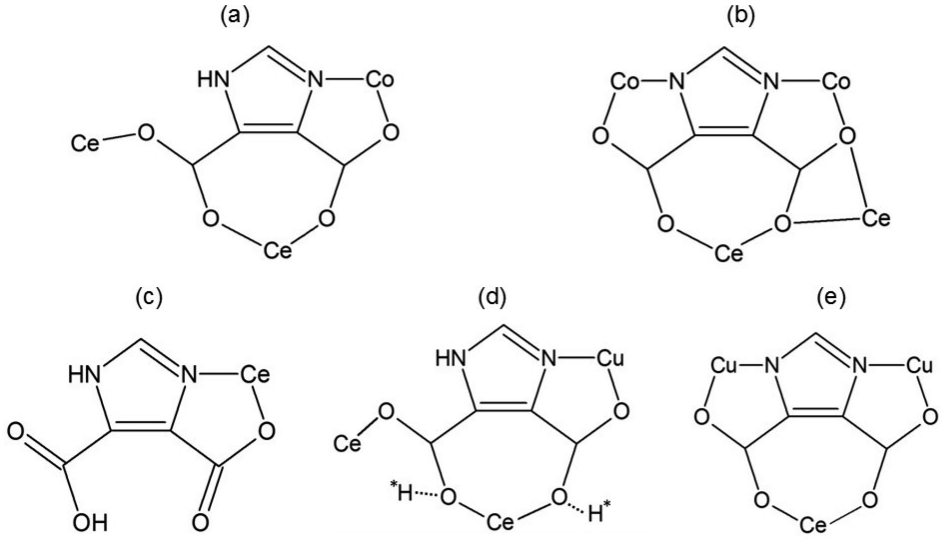

Figure 1. Coordination modes of (a) $HIDC^{2-}$, (b) IDC^{3-} in **CoCe** and (c) H_2IDC^{-}, (d) $H_{1.6}IDC^{2.4-}$, and (e) IDC^{3-} in **CuCe**. The partial hydrogen atoms from $H_{1.6}IDC^{2.4-}$ species are denoted as H*.

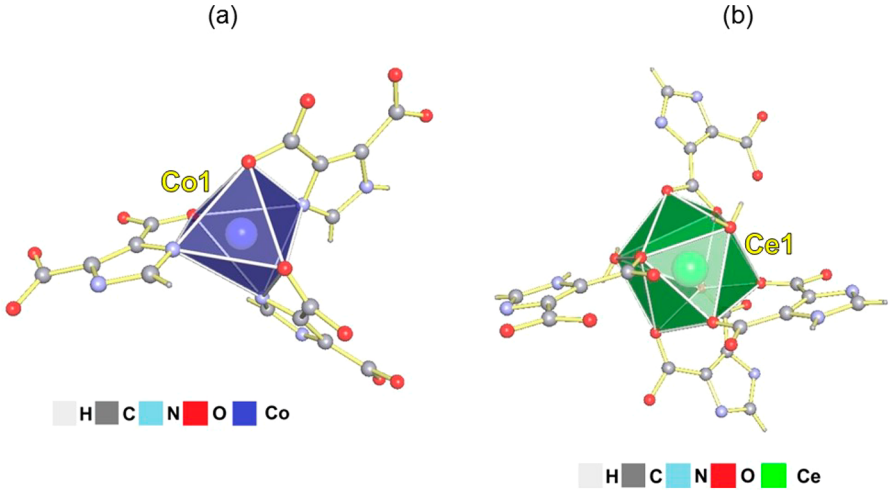

Figure 2. Coordination geometry of (a) Co1 and (b) Ce1 in **CoCe**.

used. Data were reduced by SAINT,[22] and empirical absorption corrections were applied using SADABS.[23] Single-crystal X-ray diffraction data of **CuCe** were collected at 150 K on a D8 VENTURE Bruker AXS diffractometer and processed with the APEX3 program suite,[24] also using Mo−Kα as X-ray wavelength. Frame integration and data reduction were carried out with the program SAINT,[22] and SADABS was employed for multiscan-type absorption corrections.[23]

Using the Olex2[25] package, the crystal structures were solved with the ShelXT[26] structure solution program using Dual Methods, and refined with the ShelXL[27] package using least-squares minimization based on F^2. Crystallographic data details on data collections and refinement parameters of the crystal structure are summarized in Table 1. Structure drawings have been made with TOPOs software.[28] Additional data concerning the crystals and the refinement parameters are detailed in the Supporting Information (Table S1 for **CoCe** and Table S2 for **CuCe**).

One of the coordination water molecules linked to Ce^{III} cations presents disorder (O2WA and O2WB with occupancy of 0.46 and 0.64, respectively). In addition, the solvate H_2O molecules O3W and O4W present fractional occupancy (0.3 and 0.7, respectively) and were counted as one H_2O molecule in the final formula. Finally, some hydrogen atoms in **CoCe** belonging to O2W, O3W, and O4W were not located, but were included in the reported formula of the compound.

2.4. Magnetic Measurement. Magnetic measurements were carried out using a Quantum Design Dynacool Physical Properties Measurement System (PPMS), equipped with a Vibrating Sample Magnetometer (VSM). The *dc* data were collected under external applied fields of 1−15 kOe in the 1.8−300 K temperature range.

Isothermal magnetization measurements were performed between 0 and ±90 kOe at temperatures varying from 1.8 to 8 K. Diamagnetic corrections (estimated from Pascal constants) were considered.[29] *ac* susceptibility was performed at several frequencies, with a 500 Oe dc field and 1 Oe ac oscillating field.

3. RESULTS AND DISCUSSION

3.1. Crystal Structure of $[Ce(H_2O)_2(HIDC)Co(IDC)]\cdot H_2O$ (CoCe) and $[Ce(H_2O)_2(H_2IDC)Cu(H_2O)(IDC)Cu_{0.2}(H_{1.6}IDC)]$ (CuCe). **CoCe** crystallizes in a monoclinic $P2_1/n$ space group and presents an extended framework. The asymmetric unit contains one Co^{II}, one Ce^{III} with one $HIDC^{2-}$ and IDC^{3-} anions, and three H_2O molecules. The different protonation degrees observed in the imidazole ligand can be related to the two particular coordination modes, η^3-κO-$\kappa O'$,O''-$\kappa O'''$,N and η^4-κN,O-$\kappa O'$,O''-$\kappa O''$,O'''-$\kappa O'''N'$, observed for $HIDC^{2-}$ and IDC^{3-}, respectively (Figure 1a,b). The Co^{II} centers present a

DOI: 10.1021/acs.cgd.8b00590
Cryst. Growth Des. 2018, 18, 5155−5165

distorted octahedral geometry (CoN_3O_3) with a *mer* configuration formed by two $\kappa N,O$-IDC^{3-} and one $\kappa N,O$-$HIDC^{2-}$ (Figure 2a) with d_{Co-N} and d_{Co-O} in the ranges of 2.060(5)−2.140(5) Å and 2.130(4)−2.190(4) Å, respectively (Table S1). The Ce^{III} cations present nonacoordination, formed exclusively by oxygen atoms, with d_{Ce-O} between 2.385(5) and 2.682(4) Å (Figure 2b). The geometry of the CeO_9 moiety was calculated with the SHAPE software,[30] giving a capped square antiprism (C_{4v} symmetry, J_{10} of Johnson polyhedra[31]), where the uncapped square base of the prism contains both a $HIDC^{2-}$ and IDC^{3-}, both coordinating in the $\kappa O',O''$ fashion. The capped face is occupied by two H_2O molecules in *trans* position and one $\kappa O'$-$HIDC^{2-}$ and one $\kappa O'',O'''$-IDC^{2-}, while the capped position is occupied by one of the oxygen atoms of the $\kappa O'',O'''$-IDC^{2-} carboxylate anion. (Figure S1a). One of the water molecules linked to the Ce^{III} cations presents an occupational disorder (O2W).

The 3D structure of **CoCe** can be described as formed by two independent secondary homometallic subunits, $[Ce(H_2O)_2(HIDC)]^+$ and $[Co(IDC)]^-$, as depicted in Figure 3a. By a translation and 2-fold axis, the $[Co(IDC)]^-$ fragment generates a chain along the *b* axis, in which the Co^{II} cations are connected through μ^2-$\kappa N,O$-$\kappa O''',N'$-IDC^{2-} bridges, with a Co···$Co^{\#6}$ distance of 6.160(3) Å. Moreover, these Co^{II} chains present alternating Λ or Δ helicity, generated by the presence of three chelating rings around the Co^{II} centers (Figure 3b). Nevertheless, the overall structure of **CoCe** is centrosymmetric due to an inversion center that relates both Λ and Δ chains. The Co^{II} chains are connected by Ce^{III} dinuclear discrete moieties $[Ce(H_2O)_2(HIDC)]_2^{2+}$, generating three different Ce−Co interactions by means of *anti-anti* carboxylate (Ce1···$Co1^{\#2}$ = 6.326(3) Å; Ce1···$Co1^{\#3}$ = 6.218(2) Å; Ce1···$Co1^{\#4}$ = 6.268(3) Å) and an oxocarboxylate (Ce1···$Co1^{\#5}$ = 4.741(2) Å) bridge. The isolated $[Ce(H_2O)_2(HIDC)]_2^{2+}$ moiety presents an internal Ce-Ce *syn-anti* carboxylate bridge, with a Ce1···$Ce1^{\#2}$ distance of 5.870(4) Å. Furthermore, **CoCe** presents a small interstitial space filled with H_2O molecules along the *b* axis (Figure S2).

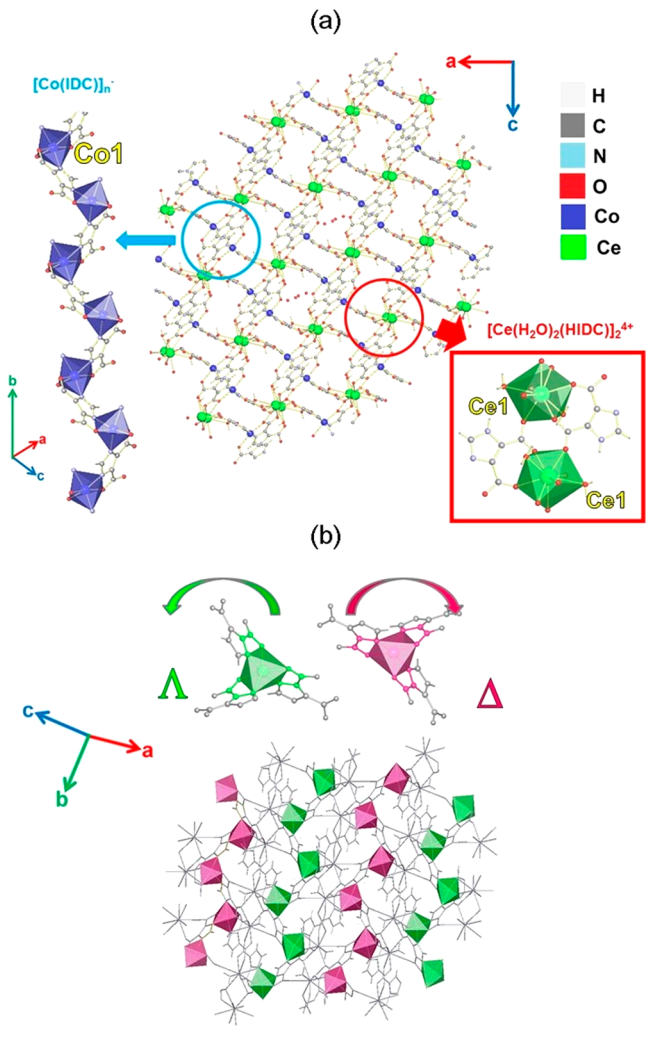

Figure 3. (a) View of the 3D extended structure of **CoCe** and (b) Co^{II} chains presenting alternating Λ or Δ helicity.

On the other hand, **CuCe** crystallizes in a monoclinic $P2_1/n$ space group and presents an extended structure with an asymmetrical unit that consists of one Ce^{III}, two different Cu^{II} cations, Cu1 and Cu2 (the latter with a fractionary occupancy of 0.2), three coordination water molecules, and different deprotonated species of H_3IDC. A diprotonated H_2IDC^- and a totally deprotonated IDC^{3-} species can be easily identified, presenting a coordination fashion of $\kappa N,O$ and η^3-κO-$\kappa O',O''$-$\kappa O'''N'$ (Figure 1c,e), respectively. An intermediate protonation degree, $H_{1.6}IDC^{1.4-}$, was detected presenting a coordination fashion of η^3-$\kappa N,O$-$\kappa O',O''$-$\kappa O'''N'$ (Figure 1d, the partial hydrogen atoms (H*) from $H_{1.6}IDC^{2.4-}$ species). The intermediate protonation degree of the ligand is a consequence of the fractional occupancy of Cu2 (which contributes with a +0.4 charge) permitting the electroneutrality of the network. Meanwhile, the hydrogen atoms with fractional occupancy were found on the carboxylate groups of $H_{1.6}IDC^{1.4-}$, similar to that in the $Co^{II}Gd^{III}$ 3D network, previously reported by our group.[32] Moreover, EDX analysis was performed to corroborate that no other cation such as K^+ is present in the sample (Figure S3), giving only signals corresponding to copper and cerium. Additionally, the $Ce^{III}Cu^{II}_{1.2}$ stoichiometry is consistent with the elemental analysis and magnetic properties.

Cu1 presents a CuN_2O_3 pentacoordination with a (4 + 1) square pyramidal geometry. The base of the pyramid is occupied by *trans* $HIDC^{2-}$ and IDC^{3-} anions, both with a $\kappa N,O$ coordination fashion, while one water molecule occupies the axial position (Figure 4a), with d_{Cu-N} of 1.959(2)−1.952(2) Å and d_{Cu-O} of 2.212(2)−1.986(2) Å (Table S2). Meanwhile, Cu2 presents a CuN_2O_2 square plane environment, reached by two trans $\kappa N,O$-IDC^{3-} anions with d_{Cu-N} of 1.942(3) Å and d_{Cu-O} of 2.000(2) Å (Table S2). Moreover, the Cu2 centers are interacting weakly in the equatorial positions with two carboxylates groups from two additional IDC^{3-} anions with a d_{Cu-O} of 2.765(2) Å ($O10^{\#1}$), giving a (4 + 2) pseudooctahedral geometry (Figure 4b). On the other hand, Ce^{III} cations present a nonacoordination with a $CeNO_8$ environment, with a d_{Ce-O} in the range of 2.4645(19)−2.6825(18) Å (average 2.54 Å) and with a d_{Ce-N} of 2.640(2) Å (Table S2). The calculated geometry with SHAPE[30] is the same to that obtained for **CoCe**, capped square antiprism (C_{4v} symmetry, J_{10} of Johnson polyhedra[31]), with the uncapped face of the prism occupied by $\kappa O',O''$-$HIDC^{2-}$ and $\kappa O',O''$-IDC^{3-}, while the capped face is formed by two *trans* H_2O molecules and two $HIDC^{2-}$ anions with two coordination modes, κO-IDC^{3-} and $\kappa N,O$-IDC^{3-}. Similar to **CoCe**, one of the oxygen belonging to the carboxylate groups of $\kappa N,O$-IDC^{3-} occupies the capped position (Figure 4c and Figure S1b). In addition,

DOI: 10.1021/acs.cgd.8b00590
Cryst. Growth Des. 2018, 18, 5155−5165

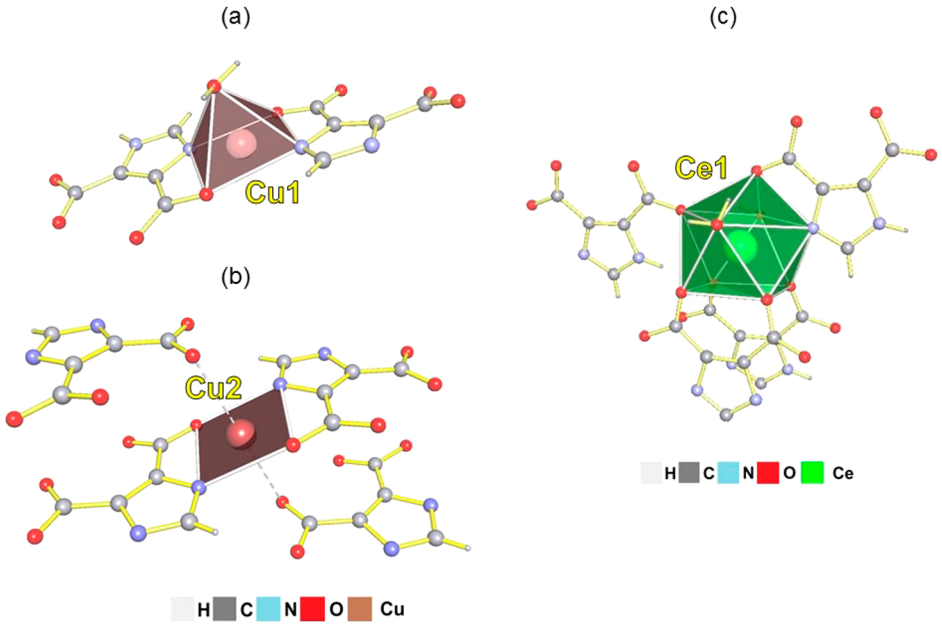

Figure 4. Coordination geometry of (a) Cu1 and (b) Cu2 and (c) Ce1 in **CuCe**.

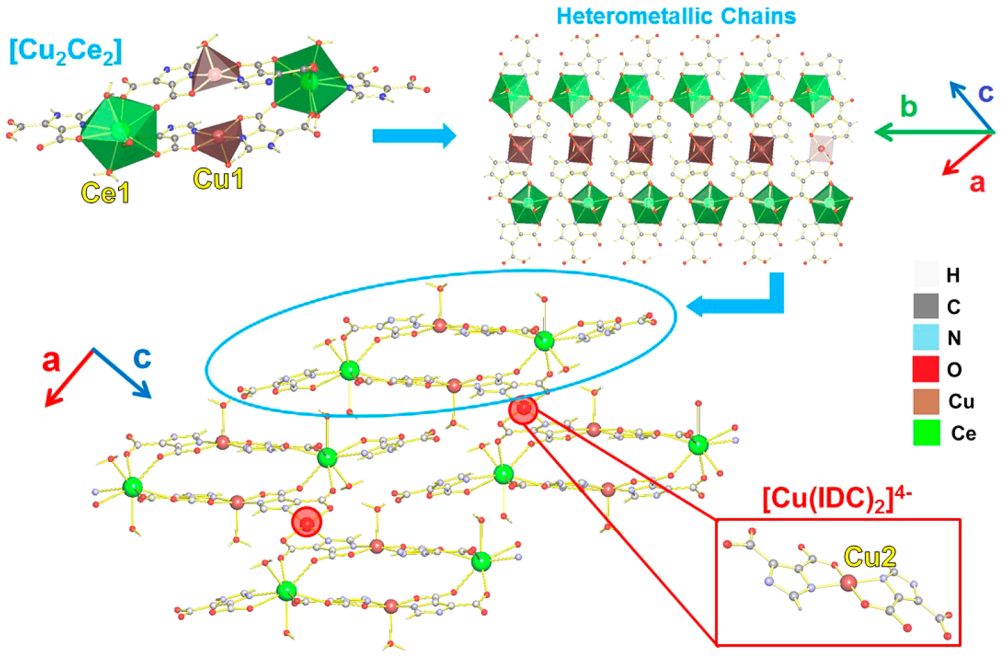

Figure 5. View of the extended structure of **CuCe**; $[Ce(H_2O)_2(H_2IDC)Cu(H_2O)(H_{1.6}IDC)(IDC)]_2^{0.4-}$ moieties labeled as [CuCe].

CuCe presents a complex extended structure depicted in Figure 5, which can be described in terms of heterometallic tetranuclear rings $[Ce(H_2O)_2(H_2IDC)Cu(H_2O)(H_{1.6}IDC)(IDC)]_2^{0.4-}$ labeled as $[Ce_2Cu_2]$, having a Cu1-Ce1-Cu1-Ce1 arrangement. The Cu-Ce connectivity of the ring is produced by two *anti-anti*-carboxylate bridges (Cu1···Ce$^{3\#}$ = 6.0128(4) Å and Cu1$^{2\#}$···Ce = 6.4998(4) Å). Furthermore, these $[Ce_2Cu_2]$ cyclic fragments are self-assembled through an *anti*/*anti*-carboxylate bridge between Ce-Ce cations (Ce1···Ce$^{1\#}$ = 6.9284(2) Å), forming a 1D substructure along the *b* axis (Figure 5). The $[Ce(H_2O)_2(H_2IDC)Cu(H_2O)(H_{1.6}IDC)(IDC)]_2^{0.4-}$ anionic 1D substructures are also partially assembled by Cu2 cations localized just between one $H_{1.6}IDC^{1.4-}$ and one IDC^{3-} anions belonging from two adjacent $[Ce_2Cu_2]$ fragments, thus reaching a 2D arrangement. This final assembly generates a Cu2−Ce bridge by means of the *anti-anti* carboxylate (Cu2···Ce1$^{4\#}$ = 6.12309(18) Å) and a Cu1−Cu2 bridge through μ^2-$\kappa N,O$-$\kappa O''',N'$-IDC^{2-} (Cu1···Cu2 = 5.9445(3) Å).

Simplification of both structures of **CoCe** and **CuCe** using TOPOs[28] (considering the metal centers as nodes and the contraction of ligands to their centroids as linkers) allows a better visualization of the topologies of the framework. In **CoCe** (Figure 6a), it is possible to observe the parallel helical $[Co(IDC)]^-$ substructures (blue sticks) that are related to each other by an inversion center. Meanwhile, in green, the $[Ce(H_2O)_2(HIDC)]_2^{2+}$ moieties are connecting the Co-chains, to achieve the 3D extended structure, in which

DOI: 10.1021/acs.cgd.8b00590
Cryst. Growth Des. 2018, 18, 5155−5165

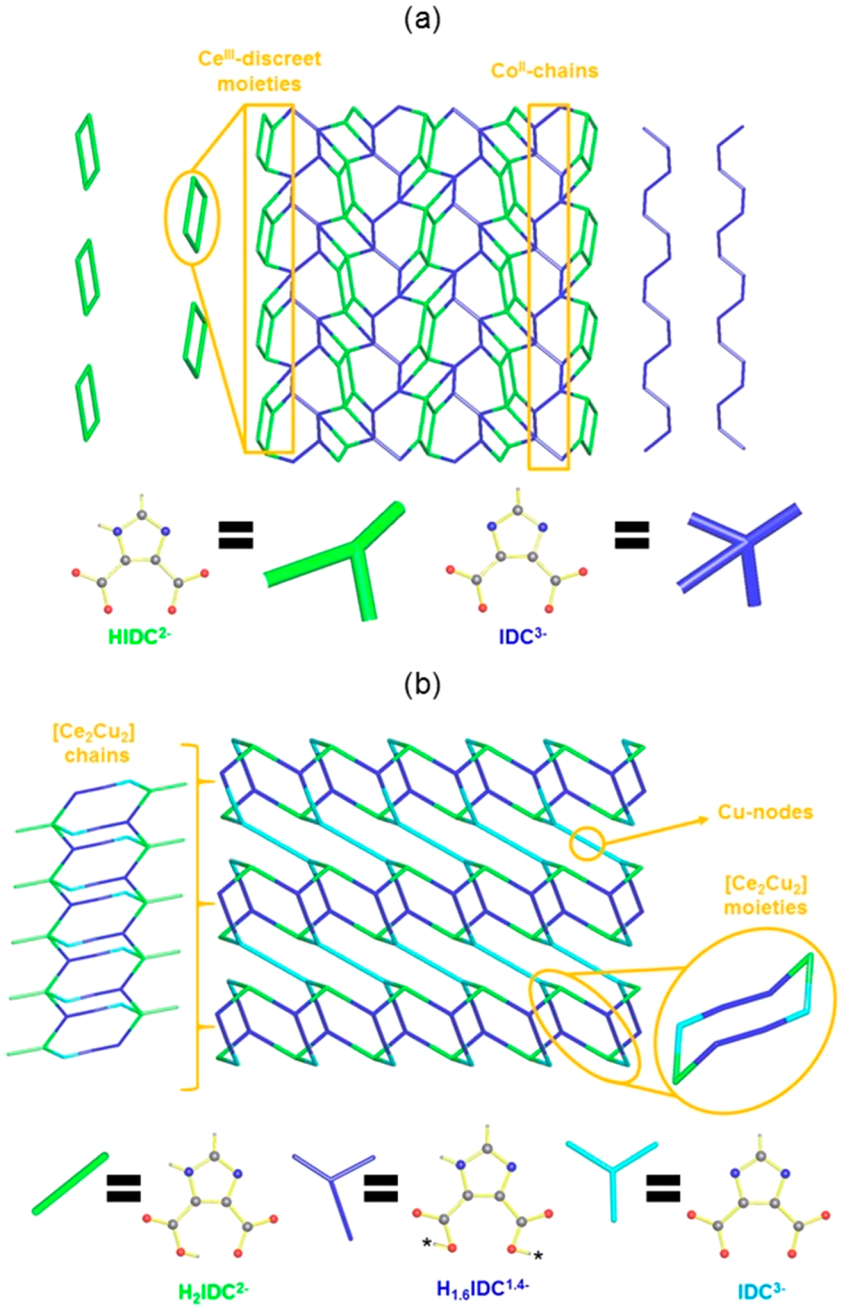

Figure 6. Simplified structural schemes of (a) **CoCe** and (b) **CuCe** using TOPOs.

$HIDC^{2-}$ and IDC^{3-} are behaving as tritopic and tetratopic linkers. On the other hand, Figure 6b shows the $[Ce_2Cu_2]$ moieties (blue-green sticks) forming the 1D heterometallic substructure connected by the Cu2 nodes (light blue sticks). In **CuCe**, both $H_{1.6}IDC^{1.4-}$ and IDC^{3-} species are behaving as tritopic linkers, and the diprotonated H_2IDC^{2-} act as the blocking ligand of the Ce^{III} cations, thus preventing the growth of the structure in this direction.

Remarkably, herein we report the synthesis of two new 3*d*-4*f* heterometallic coordination polymers (HCP) based on Ce^{III} and two different 3*d* cations, Co^{II} or Cu^{II}, by using a single organic linker, the bifunctional ligand 1*H*-imidazole-4,5-dicarboxilyc acid (H_3IDC). H_3IDC has proven to be an excellent ligand to construct coordination polymers with intricate and beautiful structures, using different metals cations such as from *n*s block,[33−35] 3*d*,[36−39] and 4*d* transition cations[40,41,42] and with lanthanide cations.[43,44] The versatility of this ligand also relies on the multiple anionic species that can be generated: H_2IDC^-, $HIDC^{2-}$, and IDC^{3-}, which not only allows the balance of charges of the cations but also gives multiple coordination sites with different coordination capabilities. Nevertheless, 3*d*-4*f* HCPs using this ligand as organic linker are still scarce. In our previous work, we used H_3IDC, in addition with oxalate as coligand, to create intricate 3D Co^{II}-Gd^{III}[32] and 2D Cu^{II}-Gd^{III} networks.[45] In this work, **CoCe** and **CuCe** were constructed only by H_3IDC anionic derivatives. From a synthetic point of view, compound **CoCe** was obtained in a one pot hydrothermal synthesis, whereas **CuCe** was obtained in a two-step synthesis using **Cu1** as metalloligand. The one pot synthesis dominates the preparation of 3*d*-4*f* HCP, while assembly of complexes using solvo/hydrothermal synthesis to obtain HCP has not been frequently

DOI: 10.1021/acs.cgd.8b00590
Cryst. Growth Des. 2018, 18, 5155−5165

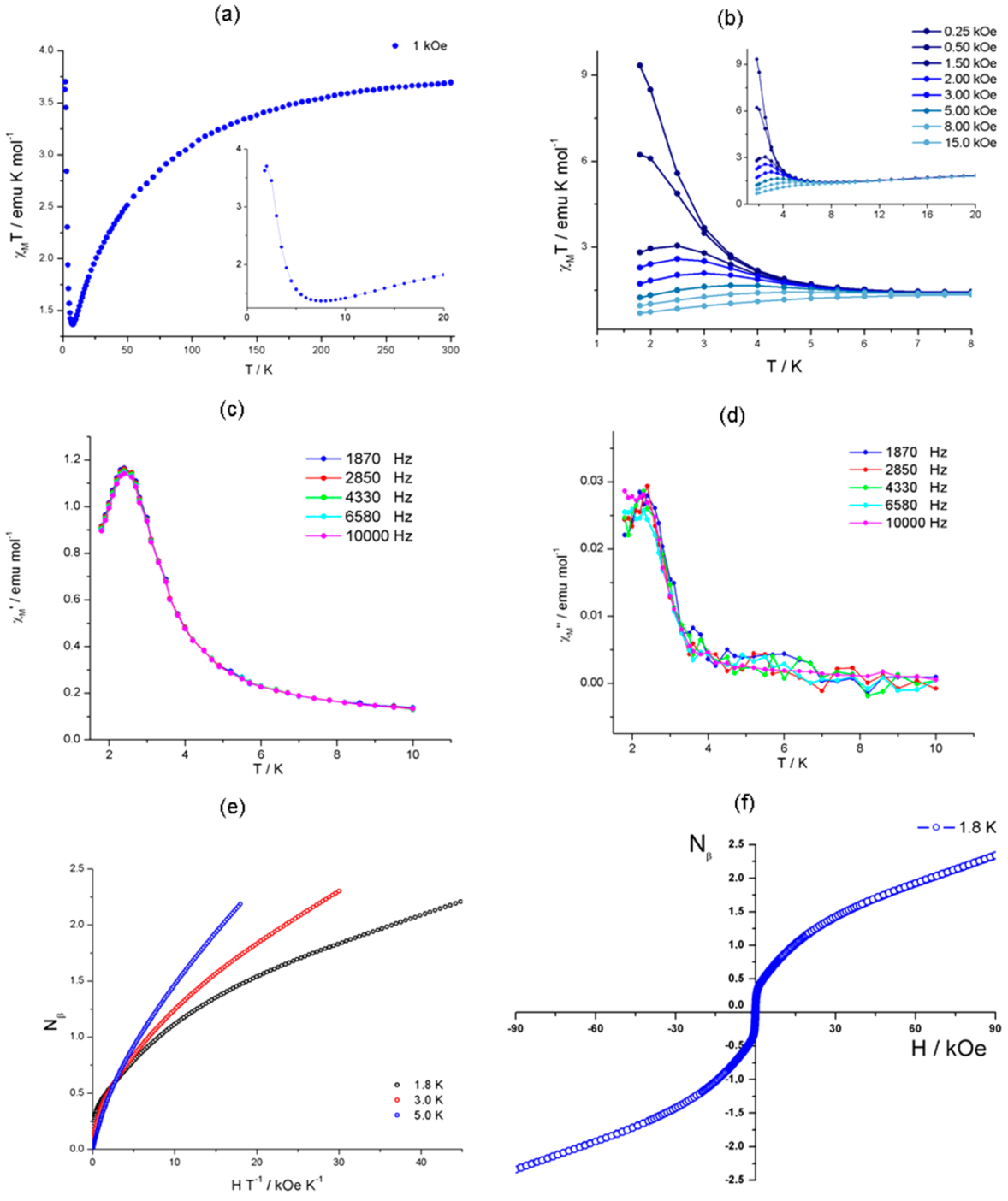

Figure 7. For compound **CoCe**: $\chi_M T$ vs T plots (a) from 300 to 1.8 K at 1 kOe and (b) from 10 to 1.8 K at several applied fields from 0.25 to 15 kOe; (c) in-phase and (d) out-of-phase *ac* susceptibility at five different frequencies; (e) N_β vs HT^{-1} magnetization plots at 1.8, 3, 5, and 8 K and (f) 1.8 K isothermal hysteresis curve.

used. For instance, using a cobalt 0D binuclear building block $[Co_2(H_2TTHA)(H_2O)_2]$ or 1D $[Co(Pzdc)_2]$ precursor, the syntheses of two different 3D HCPs $[Ce_2Co(Pzdc)_4(H_2O)_6]\cdot 2H_2O$ and $[Ce(H_2O)_4Co_2(TTHA)(SCN)_2]\cdot H_3O^+$ (H_2Pzdc = pyrazine-2,3-dicarboxylic acid; H_6TTHA = triethylenetetraaminehexaacetic) were reported.[46,47] Additionally, Gao et al. reported the synthesis of the 2D HCPs $[Ce_2Co_3(EDTA)_3(H_2O)_{11}]\cdot 12H_2O$, using in this case a 4*f* metalloligand $Na[Ce(EDTA)]\cdot 2H_2O$ (EDTA = ethylenediamine-*N*,*N*,*N*′,*N*′-tetraacetate).[48] Regarding the one pot methodology, Lio et al. reported the synthesis of $[Ce_2Co(tia)_4(H_2O)_4]$ 3D HCPs (H_2tia = 5-(1H-1,2,3-triazol-1-yl)isophthalatic acid) by the hydrothermal route.[49] Furthermore, several HCPs based on Cu^{II} and Ce^{III}, using a wide variety of organic acids, such as nicotinic,[50] iminodiacetic,[51] oxidiacetic,[52] and 1,2,4,5-benzenetetracarboxylic acids,[53] or some bifuntional ligands, such as piridin-2,6-dicarboxylic[54] and pirazin-2,3-dicarboxylic[55] acid, have been reported. However, to the best of our knowledge, Cu^{II}-Ce^{III} or Co^{II}-Ce^{III} HCP, using H_3IDC as an organic linker, has not been yet reported. Additionally, one of the most interesting features of the structure of **CoCe** is the presence of chiral Co^{II}-based chains within the 3D structure. The three

DOI: 10.1021/acs.cgd.8b00590
Cryst. Growth Des. 2018, 18, 5155−5165

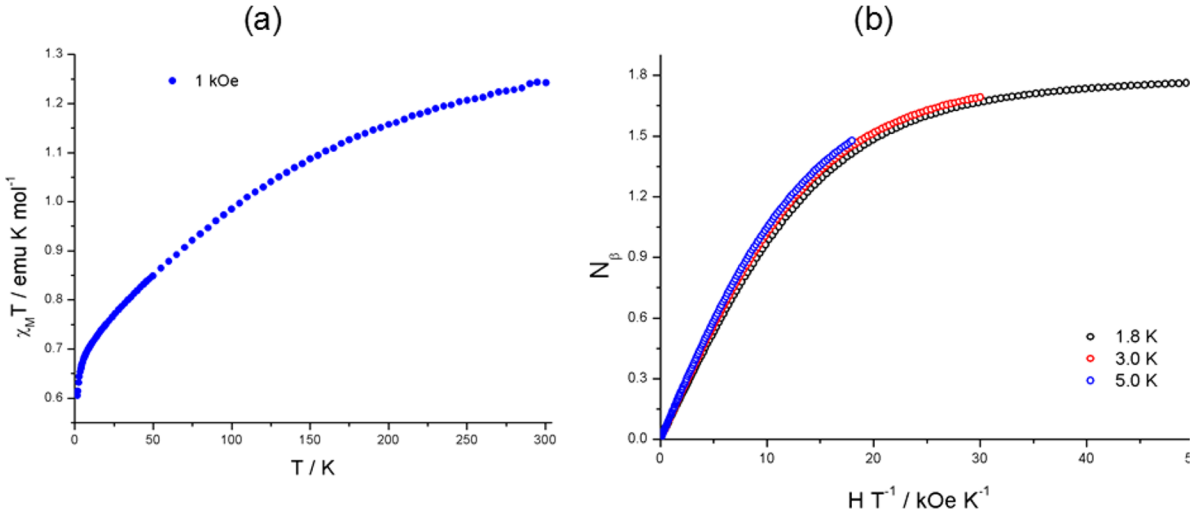

Figure 8. For **CuCe**: (a) $\chi_M T$ vs T plot from 300 to 1.8 K at 1 kOe and (b) isothermal N_β vs HT^{-1} magnetization plots at 1.8, 3, 5, and 8 K.

chelating rings generated by the $\kappa N,O$ coordination of the IDC^{3-} and $HIDC^{2-}$ species give rise to either the Λ or Δ arrangement, which produces chirality in the chains. Thus, imidazole-dicarboxylic acid derivatives are well-known to generate chiral structures like Mn^{II}, Cd^{II}, and Zn^{II} coordination polymers.[56,57] Nevertheless, achiral coordination polymers with chiral substructures are not easy to find. Li et al. reported Λ and Δ helical Co^{II}-based chains in the $[Co(HPPhIDC)(CH_3OH)]_n$ framework, using the H_3IDC homologous ligand 2-(*p*-isopropylphenyl)-1*H*-imidazole-4,5-dicarboxylic acid (H_2-PPhIDC).[58] Moreover, the two 3D 3*d*-4*f* HCP based on Co^{II} and Gd^{III} that we previously reported present the same Co^{II} chiral chain arrangement, as that observed in **CoCe**.[32] As far as we know, the two previously reported Co^{II}-Gd^{III} 3D frameworks,[32] together with **CoCe** reported in this work, are the unique examples of 3*d*-4*f* heterometallic coordination polymer containing this kind of homometallic chiral substructures as part of a 3D heterometallic network.

3.2. Magnetic Properties. Figure 7a and Figure S4a show the $\chi_M T$ vs T and $\chi_M{}^{-1}$ vs T plots for **CoCe** between 300 and 1.8 K at 1 kOe. Compound **CoCe** follows the Curie–Weiss law between 300 and 50 K, with C = 4.11 emu·mol^{-1} and θ = −31.8 K. A $\chi_M T$ product of 3.70 emu·K·mol^{-1} is observed at room temperature, which is higher than 2.68 emu·K·mol^{-1}, expected for a noninteracting Co^{II} (S = 3/2; g = 2.0) and Ce^{III} (L = 3; g = 6/7). This higher value is attributed to the strong anisotropy present in the Co^{II} cation with a high-spin configuration and a distorted O_h geometry. As the temperature is lowered from 300 K, the $\chi_M T$ values decrease monotonously to a minimum value of 1.37 emu·K·mol^{-1} at 7.5 K. Clearly, the negative value of the Weiss constant and the decrease of $\chi_M T$ with the lowering of temperature suggest that an overall antiferromagnetic behavior is present in **CoCe**. Nevertheless, from 7.5 K, an increase of $\chi_M T$ can be observed as the temperature is decreased, reaching a maximum value of 3.70 emu·K·mol^{-1} at 2 K, suggesting a ferromagnetic behavior below 7.5 K. Furthermore, Figure 7b shows $\chi_M T$ vs T plots at several applied fields (0.25–15 kOe) in a temperature range of 1.8–8 K, showing that the ferromagnetic behavior becomes more evident at lower applied fields. The *ac* susceptibility (Figure 7c,d) is in agreement with the *dc* measurement, showing a well-defined frequency independent maximum near 2.4 K for $\chi_M{}'$ and $\chi_M{}''$ components. ZFC and FC measurements at 50 Oe (Figure S4b) show a complete reversibility until 2 K. However, a small difference in the $\chi_M T$ value was observed at 1.8 K, being 9.87 and 10.5 emu·K·mol^{-1} for ZFC and FC, respectively. Additionally, isothermal field dependent magnetization measurements were performed for **CoCe**. The curves of N_β vs HT^{-1} measured at 1.8, 3, 5, and 8 K are not superimposed in a master curve (Figure 7e), confirming that the higher value of $\chi_M T$ at room temperature for **CoCe** is due to the presence of the anisotropy typical of the paramagnetic centers. Furthermore, N_β vs H hysteresis loop (Figure 7f, Figure S4c) show an S-shaped plot for **CoCe**, thus indicating that the saturation was not reached, giving a maximum value of 2.3 N_β at 90 kOe, which is less than the expected value for four electrons belonging to one Co^{II} and one Ce^{III} (d^7 high spin and f^1 electrons). The isothermal magnetization plots permit one to infer that the observed decrease of the $\chi_M T$ values can be attributed to the antiferromagnetic coupling between the paramagnetic centers and also by the strong spin–orbit contribution belonging mainly from the high-spin Co^{II} cation in a distorted O_h geometry.[59] On the other hand, the frequency independent maximum of the in-phase ($\chi_M{}'$) and out-of-phase ($\chi_M{}''$) signals, together with the irreversibility in the ZFC-FC measurements and the S shape of the hysteresis loop, can be associated with a weak ferromagnetic behavior as the product of noncompensated antiferromagnetic coupling.[60,61]

Figure 8a and Figure S4d depict $\chi_M T$ vs T and $\chi_M{}^{-1}$ vs T plots between 300 and 1.8 K for **CuCe** at 1 kOe. Compound **CuCe** follows the Curie–Weiss law between 300 and 100 K, with C = 1.42 emu·mol^{-1} and θ = −45.7 K. The $\chi_M T$ value at 300 K for this compound is 1.21 emu·K·mol^{-1}, which is very near to the expected $\chi_M T$ value for noninteracting Ce^{III} and 1.2 Cu^{II} cations (1.24 emu·K·mol^{-1} considering J_{Ce} = 5/2; g_{Ce} = 6/7; S_{Cu} = 1/2; g_{Cu} = 2.00), confirming the $Cu_{1.2}Ce$ ratio discussed in the structural section. As the temperature is lowered from 300 K, $\chi_M T$ also decreases sharply to a minimum value of 0.59 emu·K·mol^{-1} at 1.8 K. This decrease of $\chi_M T$ in the whole temperature range, in addition to the negative value of θ in $\chi_M{}^{-1}$ vs T plot, can be associated with antiferromagnetic interactions between the paramagnetic centers in **CuCe**. On the other hand, N_β vs HT^{-1} plot at 1.8 K (Figure 8b) shows that saturation is not reached, giving a value of 1.76 N_β at 90 kOe, which is rather far from the expected value for

DOI: 10.1021/acs.cgd.8b00590
Cryst. Growth Des. 2018, 18, 5155–5165

noninteracting Ce^{III} and 1.2 Cu^{II} cations (2.2 N_β considering g_{Ce} = 6/7 and g_{Cu} = 2.00). In addition, the field dependent magnetization of **CuCe** obtained at different temperatures shows a very low orbital contribution attributed to the presence of Ce^{III} cations, since Cu^{II} is magnetically isotropic.

Remarkably, the inclusion of 3*d* and 4*f* cations into intricated frameworks presents a challenge in the rational correlation between structures and magnetic phenomena. In this sense, the chemical connectivity between the paramagnetic ions is an important feature for the analysis of the magnetic properties in 3*d*-4*f* HCPs. Since 4*f* orbitals are shielded by more external orbitals, the superexchange coupling through organic bridges between 3*d*-4*f* is expected to be less in magnitude than the interaction between 3*d*-3*d* spin carriers.[13] As a consequence, the interaction between 3*d*/3*d* orbitals is expected to be stronger than that of 3*d*/4*f* and 4*f*/4*f* orbitals. As stated in the structural description section, **CoCe** and **CuCe** exhibit a wide variety of chemical bridges (Figure S5a,b) between the paramagnetic centers, making possible the interaction between Ce-Ce and Ce-3*d* cations by means of carboxylate groups belonging to H_3IDC anionic species. However, the more important interactions should be expected between 3*d*-3*d* cations through the μ^2-$\kappa N,O$-$\kappa O''',N'$-IDC^{2-} bridges, which are known as mediators of antiferromagnetic interactions.[62,63]

Cao et al.[64] and Li et al.[58] reported the magnetic properties of 3D networks having Co^{II} and the μ^2-$\kappa N,O$-$\kappa O''',N'$ bridge, but belonging to *p*-methoxyphenyl-1*H*-imidazole-4,5-dicarboxylate[64] or 2-*p*-isopropylphenyl-imidazoledicarboxylate[58] organic ligands, respectively. In both cases, antiferromagnetic interactions were established between these transition metal cations. Furthermore, Massoud et al. found the same type of magnetic interaction between Cu^{II} cations linked by μ^2-$\kappa N,O$-$\kappa O''',N'$ bridges belonging to the H_3IDC ligand, but now being part of a binuclear compound.[63] These facts permit us to assess that the predominant magnetic behavior in **CoCe** and **CuCe** is produced mainly by the superexchange interactions between the 3*d* cations. Nevertheless, Kahn et al. reported the magnetic coupling between Cu^{II}-4*f* ions in a 1D isostructural Cu^{II}-Ln^{III} series.[65] The author found that magnetic interactions between Cu^{II} and Ln^{III} depend on the electronic configuration of the 4*f* cations, being antiferromagnetic for Ce^{III} to Eu^{III} and ferromagnetic for Gd^{III} to Lu^{III}.[65] Therefore, in our case, the Cu-Ce interactions through carboxylate bridges can be expected to contribute to the bulk antiferromagnetic behavior observed for **CuCe**. In contrast, the nonisotropic character of the Co^{II} cations produces difficulties in the correlation of the corresponding magnetic properties, especially if 4*f* cations are present. However, taking into account the information reported for Co^{II} cations, both the antiferromagnetic behavior at high temperature and the weak ferromagnetism below 7.5 K observed for **CoCe** can be mainly attributed to interactions of the Co^{II} cations. It is important to note that a weak ferromagnetism emerging from an antiferromagnetic coupled system can be originated by the nonperfect antiparallel arrangement between spins carriers,[66] as stated by Shao et al., for $[Fe(LN_5)(CN)_2]$ (LN_5 = 2,13-dimethyl-3,6,9,12-tetraaza-1(2,6)pyridinacyclotridecaphane-2,12-diene). In this 1D compound, the iron pentagonal bipyramids are tilted to each other in the cyano-Fe^{II} chains, which leads to a weak ferromagnetism at low temperatures.[67] In the case of **CoCe**, the subtle deviations observed in the cobalt octahedra along the Co^{II}-chains (Figure S6a,b), can be responsible for the weak ferromagnetic behavior mentioned above.

4. CONCLUSIONS

Two new heterometallic coordination polymers based on Ce^{III} and two different 3*d* cations, Co^{II} and Cu^{II}, and the bifunctional ligand 1*H*-imidazole-4,5-dicarboxylic acid (H_3IDC) were successfully synthesized by two different synthetic approaches. The anionic species derived from the H_3IDC ligand probed to be excellent organic linkers to prepare heterometallic 3*d*-4*f* coordination polymers, with interesting structural features. **CoCe** presents a 3D coordination network, with alternated Δ-Λ chiral Co^{II}-chains substructures, generated from an achiral synthetic medium. Meanwhile, the 2D **CuCe** contains $[Cu_2Ce_2]$ heterometallic moieties assembled by partially occupied Cu^{II} cations. On the other hand, magnetic properties of **CoCe** and **CuCe** reveal antiferromagnetic behavior in both cases, but with the presence of a weak ferromagnetic behavior in **CoCe**. Considering the reported magnetic data, it is possible to infer that the role of the Ce^{III} cation is rather innocent from a magnetic point of view, being the magnetic properties dominated by the 3*d* cations. However, the lanthanide cations are essential for the construction of these two heterometallic networks. Remarkably, the inclusion of 3*d* cations and lanthanide cations using the versatile linker 1*H*-imidazole-4,5-dicarboxylic acid offers a new potential via to the rational design of 3*d*-4*f* HCPs with novel architectures and interesting properties.

■ ASSOCIATED CONTENT

Supporting Information

The Supporting Information is available free of charge on the ACS Publications website at DOI: 10.1021/acs.cgd.8b00590.

Description of the polyhedra around Ce^{III} centers in **CoCe** and **CuCe** (Figure S1); view along *ac* plane of **CoCe** (Figure S2); SEM image and EDX analysis of **CuCe** (Figure S3); χ_M^{-1} vs *T*, ZFC-FC measurements and inset hysteresis loop for **CoCe**, χ_M^{-1} vs *T* measurements for **CuCe** (Figure S4); magnetic pathways for **CoCe** and **CuCe** (Figure S5); scheme of spins arrangement in the Co^{II}-based chains in **CoCe** and Co^{II}-imidazole-Co^{II} moiety (Figure S6); experimental and simulated single crystal PXRD for **CuCe** and **CoCe** (Figure S7) (PDF)

Accession Codes

CCDC 1832094−1832095 contain the supplementary crystallographic data for this paper. These data can be obtained free of charge via www.ccdc.cam.ac.uk/data_request/cif, or by emailing data_request@ccdc.cam.ac.uk, or by contacting The Cambridge Crystallographic Data Centre, 12 Union Road, Cambridge CB2 1EZ, UK; fax: +44 1223 336033.

■ AUTHOR INFORMATION

Corresponding Author

*E-mail: vparedes@unab.cl. Tel: +56-2-2661 5756.

ORCID

Diego Venegas-Yazigi: 0000-0001-7816-2841

Verónica Paredes-García: 0000-0002-7537-7430

Notes

The authors declare no competing financial interest.

DOI: 10.1021/acs.cgd.8b00590
Cryst. Growth Des. 2018, 18, 5155−5165

■ ACKNOWLEDGMENTS

The authors acknowledge FONDECYT 1170887, Proyecto Anillo CONICYT ACT 1404 grant, CONICYT-FONDEQUIP/PPMS/EQM130086-UNAB, Chilean-French International Associated Laboratory for Multifunctional Molecules and Materials-LIAM3-CNRS No.1027 and ECOS/CONICYT C15E02. The authors acknowledge CEDENNA, Financiamiento Basal, FB0807. The authors also acknowledge the support of the Laboratory of Analyses of Solids (L.A.S-UNAB).

■ REFERENCES

(1) Zheng, K.; Liu, Z. Q.; Huang, Y.; Chen, F.; Zeng, C. H.; Zhong, S.; Ng, S. W. Highly Luminescent Ln-MOFs Based on 1,3-Adamantanediacetic Acid as Bifunctional Sensor. *Sens. Actuators, B* **2018**, *257*, 705−713.

(2) Liuzzo, V.; Oberhauser, W.; Pucci, A. Synthesis of New Red Photoluminescent Zn (II)-Salicylaldiminato Complex. *Inorg. Chem. Commun.* **2010**, *13*, 686−688.

(3) Cao, C.; Liu, S. J.; Yao, S. L.; Zheng, T. F.; Chen, Y. Q.; Chen, J. L.; Wen, H. R. Spin-Canted Antiferromagnetic Ordering in Transition Metal-Organic Frameworks Based on Tetranuclear Clusters with Mixed V- and Y-Shaped Ligands. *Cryst. Growth Des.* **2017**, *17*, 4757−4765.

(4) Feng, F.; Guo, N.; Chen, H.; Wang, H.; Yue, L.; Chen, X.; Ng, S. W.; Liu, X.; Ma, L.; Wang, L. A Series Anionic Host Coordination Polymers Based on Azoxybenzene Carboxylate: Structures, Luminescence and Magnetic Properties. *Dalton Trans.* **2017**, *46*, 14192−14200.

(5) Liang, H.; Jiao, X.; Li, C.; Chen, D. Flexible Self-Supported Metal-Organic Frameworks Mats with Exception High Porosity for Enhanced Separation and Catalysis. *J. Mater. Chem. A* **2018**, *6*, 334−341.

(6) Hiraide, S.; Tanaka, H.; Ishikawa, N.; Miyahara, M. T. Intrinsic Thermal Management Capabilities of Flexible Metal- Organic Frameworks for Carbon Dioxide Separation and Capture. *ACS Appl. Mater. Interfaces* **2017**, *9*, 41066−41077.

(7) Castaldelli, E.; Jayawardena, K. D. G. I.; Cox, D. C.; Clarkson, G. J.; Walton, R. I.; Le-Quang, L.; Chauvin, J.; Silva, S. R. P.; Demets, G. J. F. Electrical Semiconduction Modulated by Light in a Cobalt and Naphthalene Diimide Metal-Organic Framework. *Nat. Commun.* **2017**, *8*, 2139.

(8) Ryu, M.; Lee, Y. A.; Jung, O. S. Rigid 2D Networks of Copper (II) Complexes Containing Diallylbis (Pyridin-3-Yl)Silane: Insight into Anion and Media Effects on Catechol Oxidation Catalysis. *J. Mol. Struct.* **2018**, *1152*, 321−327.

(9) Jin, H. G.; Hong, X. J.; Tan, H.-C.; Wei, Q.; Lin, X. M.; Cai, Y. P. Achiral Aromatic Solvent-Induced Assemblies of the 3-D Homochiral Porous 3d-4f Heterometallic-Organic Frameworks Based on Isonicotinic Acid. *CrystEngComm* **2017**, *19*, 5956−5959.

(10) Yang, T. H.; Silva, A.; Fu, L.; Shi, F. N. Synthesis, Crystal Structure and Catalytic Property of Porous 3d−4f Heterometallic Coordination Polymers Constructed from Pyrazine-2,3- Dicarboxylic Acid. *Z. Anorg. Allg. Chem.* **2017**, *643*, 1801−1808.

(11) Zhang, X.; Chen, C.; Liu, X.; Gao, P.; Hu, M. Series of Chiral Interpenetrating 3d−4f Heterometallic MOFs : Luminescent Sensors and Magnetic Properties. *J. Solid State Chem.* **2017**, *253*, 360−366.

(12) Andruh, M.; Costes, J.; Diaz, C.; Gao, S. 3d-4f Combined Chemistry: Synthetic Strategies and Magnetic Properties. *Inorg. Chem.* **2009**, *48*, 3342−3359.

(13) Benelli, C.; Gatteschi, D. Magnetism of Lanthanides in Molecular Materials with Transition-Metal Ions and Organic Radicals. *Chem. Rev.* **2002**, *102*, 2369−2387.

(14) Zhang, S.; Cheng, P. Recent Advances in the Construction of Lanthanide-Copper Heterometallic Metal-Organic Frameworks. *CrystEngComm* **2015**, *17*, 4250−4271.

(15) Pearson, R. G. Hard and Soft Acids and Bases. *J. Am. Chem. Soc.* **1963**, *85*, 3533−3539.

(16) Fang, R.; Zhang, X. Diversity of Coordination Architecture of Metal 4,5-Dicarboxyimidazole. *Inorg. Chem.* **2006**, *45*, 4801−4810.

(17) Zhang, S.; Shi, W.; Cheng, P. The Coordination Chemistry of N-Heterocyclic Carboxylic Acid: A Comparison of the Coordination Polymers Constructed by 4,5-Imidazoledicarboxylic Acid and 1H-1,2,3-Triazole-4,5-Dicarboxylic Acid. *Coord. Chem. Rev.* **2017**, *352*, 108−150.

(18) Gu, Z.; Fang, H.; Yin, P.; Tong, L.; Ying, Y.; Hu, S.; Li, W.; Cai, Y. A Family of Three-Dimensional Lanthanide-Zinc Heterometal Organic Frameworks from 4,5-Imidazoledicarboxylate and Oxalate. *Cryst. Growth Des.* **2011**, *11*, 2220−2227.

(19) Zhao, X.; Ye, X.; Chang, L.; Wei, Z.; Liu, W.; Yue, S.; Liu, Y.-L.; Mo, H.-H.; Cai, Y.-P. Two Novel 3D Microporous Heterometallic 3d − 4f Coordination Frameworks with Unique (7,8)-Connected Topology: Synthesis, Crystal Structure and Magnetic Properties. *Inorg. Chem. Commun.* **2012**, *16*, 95−99.

(20) Yue, S.; Wei, Z.; Wang, N.; Liu, W.; Zhao, X.; Chang, L.; Liu, Y.; Mo, H.; Cai, Y. Three Novel Microporous 3D Heterometallic 3d − 4f Coordination Polymers: Synthesis, Crystal Structures and Photoluminescence Properties. *Inorg. Chem. Commun.* **2011**, *14*, 1396−1399.

(21) Li, S. M.; Zheng, X. J.; Yuan, D. Q.; Ablet, A.; Jin, L. P. In Situ Formed White-Light-Emitting Lanthanide-Zinc-Organic Frameworks. *Inorg. Chem.* **2012**, *51*, 1201−1203.

(22) *SAINT V6.22*; Bruker AXS Inc.: Madison, WI, 2000.

(23) *SADABS V2.05*; Bruker AXS Inc.: Madison, WI, 2001.

(24) *APEX3 V2016.1-0*; Bruker AXS Inc.: Wisconsin, USA, 2016.

(25) Dolomanov, O. V.; Bourhis, L. J.; Gildea, R. J.; Howard, J. A. K.; Puschmann, H. OLEX2: A Complete Structure Solution, Refinement and Analysis Program. *J. Appl. Crystallogr.* **2009**, *42*, 339−341.

(26) Sheldrick, G. M. SHELXT - Integrated Space-Group and Crystal-Structure Determination. Acta Crystallogr. *Acta Crystallogr., Sect. A: Found. Adv.* **2015**, *71*, 3−8.

(27) Sheldrick, G. M. Crystal Structure Refinement with SHELXL. *Acta Crystallogr., Sect. C: Struct. Chem.* **2015**, *71*, 3−8.

(28) Blatov, V.; Shevchenko, A. *ToposPro: Program Package for Multipurpose Crystallochemical Analysis*; ToposPro: Samara, Russia, 2014.

(29) Bain, G. A.; Berry, J. F. Diamagnetic Corrections and Pascal's Constants. *J. Chem. Educ.* **2008**, *85*, 532−536.

(30) Llunell, M.; Casanova, D.; Cirera, J.; Bofill, J.; Alemany, P.; Alvarez, S.; Pinsky, M.; Avnir, D. *SHAPE V2.1*; Universitat de Barcelona: Barcelona, Spain, 2013. (This program has been developed in the group of Prof. Alvarez at the Universitat de Barcelona and is available from the authors: atllunell@qf.ub.es.)

(31) Johnson, N. Convex Polyhedra with Regular Faces. *J. Can. Mathématiques* **1966**, *18*, 169−200.

(32) Cruz, C.; Spodine, E.; Vega, A.; Venegas-Yazigi, D.; Paredes Garcia, V. Novel 3d/4f Metal Organic Networks Containing Co(II) Chiral Chains. *Cryst. Growth Des.* **2016**, *16*, 2173−2182.

(33) Zhong, R.; Zou, R.; Du, M.; Takeichi, N.; Xu, Q. Observation of Helical Water Chains Reversibly Inlayed in Magnesium Imidazole-4,5-Dicarboxylate. *CrystEngComm* **2008**, *10*, 1175−1179.

(34) Schieber, N. P.; Combs, S.; Vakiti, R. K.; Yan, B.; Webb, C. Hydrogen-Bonded Sodium−organic Frameworks from Imidazole-4,5-Dicarboxylic Acid. *J. Coord. Chem.* **2012**, *65*, 4177−4184.

(35) Starosta, W.; Leciejewicz, J.; Premkumar, T.; Govindarajan, S. Crystal Structures of Two Ca(II) Complexes with Imidazole-4,5-Dicarboxylate and Water Ligands. *J. Coord. Chem.* **2006**, *59*, 557−564.

(36) Wen, L. L.; Wang, D. E.; Chen, Y. J.; Meng, X. G.; Li, D. F.; Lan, S. Syntheses, Crystal Structures and Luminescence of Two Isostructural Coordination Polymers Constructed from 4,5-Imidazoledicarboxylate. *J. Coord. Chem.* **2009**, *62*, 789−796.

(37) Zhang, X.; Huang, D.; Chen, F.; Chen, C.; Liu, Q. The First One-Dimensional Manganese Polymer Containing 4,5-Dicarboxyimidazole: Solvothermal Synthesis, Crystal Structure and Magnetic

DOI: 10.1021/acs.cgd.8b00590
Cryst. Growth Des. 2018, 18, 5155−5165

Behavior of [Mn(Phen)(Hdcbi)]n (H3dcbi = 4,5-Dicarboxyimidazole, Phen = 1,10-Phenanthroline). *Inorg. Chem. Commun.* **2004**, *7*, 662−665.
(38) Hu, T.; Bi, W.; Hu, X.; Zhao, X.; Sun, D. Construction of Metal-Organic Frameworks with Novel {Zn8O13} SBU or Chiral Channels through in Situ Ligand Reaction. *Cryst. Growth Des.* **2010**, *10*, 3324−3326.
(39) Alkordi, M. H.; Brant, J.; Wojtas, L.; Kravtsov, V. C.; Cairns, A. J.; Eddaoudi, M. Zeolite-like Metal- Organic Frameworks (ZMOFs) Based on the Directed Assembly of Finite Metal- Organic Cubes (MOCs). *J. Am. Chem. Soc.* **2009**, *131*, 17753−17755.
(40) Gu, Z. G.; Cai, Y. P.; Fang, H. C.; Zhou, Z. Y.; Thallapally, P.; Tian, J.; Liu, J.; Exarhos, G. Conversion of Nonporous Helical Cadmium Organic Framework to a Porous Form. *Chem. Commun.* **2010**, *46*, 5373−5375.
(41) Wang, X.; Qin, C.; Wang, E.; Xu, L. New One-Dimensional Imidazole-Bridged Cadmium(II) Coordination Polymers-Syntheses, Crystal Structures and Photoluminescence. *J. Mol. Struct.* **2005**, *749*, 45−50.
(42) Zhao, B.; Zhao, X. Q.; Shi, W.; Cheng, P. Synthesis, Structure and Luminescent Property of a 2D Polymer Containing Silver Ions. *J. Mol. Struct.* **2007**, *830*, 143−146.
(43) Lu, W. G.; Jiang, L.; Lu, T. B. Lanthanide Contraction and Temperature-Dependent Structures of Lanthanide Coordination Polymers with Imidazole-4,5-Dicarboxylate and Oxalate. *Cryst. Growth Des.* **2010**, *10*, 4310−4318.
(44) Li, Z.; Zhang, Z.; Dai, J.; Huang, H.; Li, X.; Yue, S.; Liu, Y. Three Novel Lanthanide Complexes with Imidazole-4,5-Dicarboxylate Ligand: Hydrothermal Syntheses, Structural Characterization, and Properties. *J. Mol. Struct.* **2010**, *963*, 50−56.
(45) Cruz, C.; Spodine, E.; Venegas-Yazigi, D.; Paredes-García, V. Cu(II)−Gd(III) 2D-Coordination Polymer Based on Two Different Organic Linkers. *Polyhedron* **2017**, *136*, 117−124.
(46) Wei, Q.; Zhang, S.; Yang, Q.; Chen, S. P.; Gong, W. J.; Zhang, Y. P.; Zhang, G. C.; Zhou, C. S.; Gao, S. L. Hydrothermal Synthesis, Structure, Magnetic, and Photoluminescent Properties of a Heterometallic Cobalt(II)/Cerium(III) Coordination Compound with the Ligand Pyrazine 2, 3-Dicarboxylic Acid. *Z. Anorg. Allg. Chem.* **2013**, *639*, 142−147.
(47) Ouyang, Y.; Xie, C. Z.; Xu, J. Y.; Yu, L.; Zhang, M. L.; Liao, D. Z. Three Cobalt (II) Complexes with Triethylenetetraaminehexaacetic Acid: From Binuclear Complex to 3d-4f Coordination Polymers. *Inorg. Chem. Commun.* **2013**, *27*, 166−170.
(48) Gao, S.; Bai, O.; Ma, B.; Yi, T.; Yan, C.; Xu, G. A Novel Two-Dimensional 4f-3d Coordination Polymer Ce2Co3(EDTA)3(H2O)-11·12H2O. *J. Chem. Crystallogr.* **2000**, *30*, 163−166.
(49) Liao, S. Y.; Gu, W.; Yang, L. Y.; Li, T. H.; Tian, J. L.; Wang, L.; Zhang, M.; Liu, X. Series of Novel 3D Heterometallic Frameworks Based on the Co(II) Coordination Chains and Ln(III) Coordination Layers. *Cryst. Growth Des.* **2012**, *12*, 3927−3936.
(50) Li, X.; Huang, Y.; Cao, R. Three-Dimensional Pillared-Layer 3d-4f Heterometallic Coordination Polymers with or without Halides. *Cryst. Growth Des.* **2012**, *12*, 3549−3556.
(51) Torres, J.; Morales, P.; Domínguez, S.; González-Platas, J.; Faccio, R.; Castiglioni, J.; Mombrú, A. W.; Kremer, C. Comparative Study of Nanoporous Ln−Cu Coordination Polymers Containing Iminodiacetate as Bridging Ligand. *J. Mol. Struct.* **2011**, *1004*, 215−221.
(52) Li, J.; Du, Z.; Huang, W. A Heterometallic Copper(II)-Cerium(III) Complex Bridged by Oxydiacetate Ligand: Synthesis, Structure, Spectral, and Magnetic Properties of {[Ce2Cu3(Oda)6-(H2O)3]·4H2O}n. *Synth. React. Inorg., Met.-Org., Nano-Met. Chem.* **2014**, *44*, 352−357.
(53) Díaz-Gallifa, P.; Fabelo, O.; Cañadillas-Delgado, L.; Pasán, J.; Labrador, A.; Lloret, F.; Julve, M.; Ruiz-Pérez, C. Synthesis, Crystal Structure and Magnetic Characterization of Series of CuII−LnIII Heterometallic [Ln= La, Ce, Pr, Nd and Sm) Metal−Organic Compounds with an Unusual Single Crystal to Single Crystal Phase Transition. *Cryst. Growth Des.* **2013**, *13*, 4735−4745.
(54) Prasad, T. K.; Rajasekharan, M. V. Heterometallic Coordination Compounds of Dipicolinic Acid with Ce(III,IV) and Cu(II): Synthesis, Crystal Structure and Spectral Studies. *Inorg. Chim. Acta* **2010**, *363*, 2971−2976.
(55) Yang, Q.; Xie, G.; Wei, Q.; Chen, S.; Gao, S. Structures and Standard Molar Enthalpies of Formation of a Series of Ln(III)-Cu(II) Heteronuclear Compounds with Pyrazine-2,3-Dicarboxylic Acid. *J. Solid State Chem.* **2014**, *215*, 26−33.
(56) Wang, W.; Niu, X.; Gao, Y.; Zhu, Y.; Li, G.; Lu, H.; Tang, M. One Chiral and Two Achiral 3-D Coordination Polymers Constructed by 2-Phenyl Imidazole Dicarboxylate. *Cryst. Growth Des.* **2010**, *10*, 4050−4059.
(57) Yang, L.; Zeng, L.; Gu, W.; Tian, J.; Liao, S.; Zhang, M.; Wei, X.; Xin, L.; Liu, X. Synthesis, Characterization and Properties of Chiral and Non-Chiral Coordination Polymers in a Zinc 2-(Pyridine-3-Yl)-1H-Imidazole-4, 5-Dicarboxylic Acid System. *Inorg. Chem. Commun.* **2013**, *29*, 76−81.
(58) Li, L.; Guo, B.-B.; Zhang, J.; Li, G. Solvothermal Synthesis, Crystal Structure and Magnetic Properties of a 3D CoII Framework Based on 2-p-Isopropylphenyl Imidazole Dicarboxylate. *Inorg. Chem. Commun.* **2013**, *36*, 86−89.
(59) Lloret, F.; Julve, M.; Cano, J.; Ruiz-García, R.; Pardo, E. Magnetic Properties of Six-Coordinated High-Spin Cobalt(II) Complexes: Theoretical Background and Its Application. *Inorg. Chim. Acta* **2008**, *361*, 3432−3445.
(60) Liu, X.; Qu, X.; Zhang, S.; Ke, H.; Yang, Q.; Shi, Q.; Wei, Q.; Xie, G.; Chen, S. High-Performance Energetic Characteristics and Magnetic Properties of a Three-Dimensional Cobalt(II) Metal-Organic Framework Assembled with Azido and Triazole. *Inorg. Chem.* **2015**, *54*, 11520−11525.
(61) Ahmad, M.; Sharma, M. K.; Das, R.; Poddar, P.; Bharadwaj, P. K. Syntheses, Crystal Structures, and Magnetic Properties of Metal − Organic Hybrid Materials of Co(II) Using Flexible and Rigid Nitrogen- Based Ditopic Ligands as Spacers. *Cryst. Growth Des.* **2012**, *12*, 1571−1578.
(62) Angaridis, P.; Kampf, J. W.; Pecoraro, V. L. Multinuclear Fe(III) Complexes with Polydentate Ligands of the Family of Dicarboxyimidazoles: Nuclearity- and Topology-Controlled Syntheses and Magneto-Structural Correlations. *Inorg. Chem.* **2005**, *44*, 3626−3635.
(63) Massoud, S. S.; Gallo, A. A.; Dartez, M. J.; Gautreaux, J. G.; Vicente, R.; Albering, J. H.; Mautner, F. A. Dinuclear Copper(II) Complexes Bridged by Imidazole-4,5-Dicarboxylate. *Inorg. Chem. Commun.* **2014**, *43*, 35−38.
(64) Cao, X.; Zhang, J.; Wang, C.; Zhu, Y.; Li, G. Design and Construction of Six Metal-Organic Frameworks with 2-p-Methoxyphenyl-1H-Imidazole-4,5-Dicarboxylate. *CrystEngComm* **2012**, *14*, 4357−4368.
(65) Kahn, M. L.; Mathonière, C.; Kahn, O. Nature of the Interaction between Ln(III) and Cu(II) Ions in the Ladder-Type Compounds {Ln(2)[Cu(Opba)](3)}.S (Ln = Lanthanide Element; Opba = Ortho-Phenylenebis(Oxamato), S = Solvent Molecules). *Inorg. Chem.* **1999**, *38*, 3692−3697.
(66) Carlin, R. L. Ferromagnetism and Anti-Ferromagnetism. In *Magnetochemistry*; Springer: Chicago, IL, 1986; Vol. 6, pp 112−162.
(67) Shao, D.; Zhang, S. L.; Zhao, X. H.; Wang, X. Y. Spin Canting, Metamagnetism, and Single-Chain Magnetic Behaviour in a Cyano-Bridged Homospin Iron(II) Compound. *Chem. Commun.* **2015**, *51*, 4360−4363.

DOI: 10.1021/acs.cgd.8b00590
Cryst. Growth Des. 2018, 18, 5155−5165